

Cavity magnon polariton based precision magnetometry

N. Crescini,^{1,2, a)} C. Braggio,^{2,3} G. Carugno,^{2,3} A. Ortolan,¹ and G. Ruoso¹

¹⁾*INFN-LNL, Viale dell'Università 2, 35020 Legnaro (PD), Italy*

²⁾*Dipartimento di Fisica e Astronomia, Via Marzolo 8, 35131 Padova, Italy*

³⁾*INFN-Sezione di Padova, Via Marzolo 8, 35131 Padova, Italy*

(Dated: 12 January 2022)

A photon-magnon hybrid system can be realized by coupling the electron spin resonance of a magnetic material to a microwave cavity mode. The quasiparticles associated with the system dynamics are the cavity magnon polaritons, which arise from the mixing of strongly coupled magnons and photons. We illustrate how these particles can be used to probe the magnetization of a sample with a remarkable sensitivity, devising suitable spin-magnetometers which ultimately can be used to directly assess oscillating magnetic fields. Specifically, the capability of cavity magnon polaritons of converting magnetic excitations to electromagnetic ones, allows for translating to magnetism the quantum-limited sensitivity reached by state-of-the-art microwave detectors. Here we employ hybrid systems composed of microwave cavities and ferrimagnetic spheres, to experimentally implement two types of novel spin-magnetometers.

Among the most studied types of hybrid systems, an important role is played by photon-magnon hybrid systems (PMHSs)^{1,2}. These yielded remarkable results in the study of light-matter interaction³, and in the last decades emerged as promising constituents for new quantum technologies as well⁴⁻⁶. PMHSs have different forms, as they are built with miscellaneous building blocks, but the underlying physics is similar. In a magnetic field B_0 , a spin can change its quantum state from $-1/2$ to a $+1/2$ by absorbing a spin-1 boson, like a photon, and vice versa by emitting one. In this sense, a quanta of spin excitation with energy $\hbar\omega_m = \mu_B B_0$ can be effectively described as a quasiparticle, known as magnon, which can turn into a photon of the same energy $\hbar\omega_c$ ⁷. This reciprocal conversion is quantified by the interaction strength g_{cm} , known as vacuum Rabi splitting, which is the rate at which magnons are converted into photons and vice versa. When g_{cm} is much larger than the damping rates of the magnon γ_m and of the photon γ_c , the system is in the strong coupling regime, and the quasiparticles arising from this mixing are known as cavity magnon polaritons (CMPs)^{8,9}.

PMHSs are widely investigated for advancing quantum information science. In this field their importance lies in building quantum memories¹⁰⁻¹⁶, in converting microwaves to optical photons¹⁷⁻²¹, or in quantum sensing, where the detection of single magnons was recently demonstrated²²⁻²⁴. CMP recently found new applications in the field of non-Hermitian physics²⁵⁻²⁷, where they already yielded outstanding results²⁸. Exceptional points, spots of the system's parameter space highly sensitive to external stimulations, can be probed with PMHSs^{29,30}, and new configurations may be designed to access more exotic phenomena and study their applications^{31,32}. The potential of hybrid systems was also shown in many other applications of quantum physics³³⁻³⁷.

A distinguished physical realisation of this model can be obtained by hybridising the microwave photons of a resonant cavity with the magnons of a ferrimagnetic insulator³⁸⁻⁴². Such scheme was implemented with multiple purposes, for example to develop new quantum tech-

nologies with qubits^{10,43}, or for microwave-to-optical photon conversion^{20,21}, making it an established platform of hybrid magnonics.

In the devices described in this letter, we employ copper cavities as a photonic resonator and Yttrium Iron Garnet (YIG) spheres as magnetic material (see Fig. 1a). YIG has the exceptionally high electron spin density of 2×10^{28} spin/m³ already at room temperature, and a linewidth as narrow as 1 MHz. This latter value is matched to the one of a typical copper cavity and, thanks to the chosen spherical shape, is not affected by geometric demagnetization. Being employed in a number of microwave and rf devices, YIG is among the most well-known ferrites, and hence is readily available. The magnetic sample is placed inside the cavity, where the rf magnetic field is maximum for the selected cavity mode, and is magnetised with a static field B_0 perpendicular to the cavity one. In this way, the Kittel mode of magnetisation couples to the microwave cavity photons, and the system exhibits the typical anticrossing dispersion relation, of which an example is shown in Fig. 1b. The coupling strength depends on the working frequency, on the microwave mode volume, and on the number of spins involved⁴⁰, but it is normally large enough to let the photon (magnon) oscillate into magnon (photon) many times before being dissipated.

This feature of CMP to be a mixed state of microwaves and spin excitations allows one to extract information on magnons by monitoring photons. In the presence of a strong coupling, the signal transduction is efficient, i. e. without signal loss, as a spin excitation is more likely converted to a photon and detected, than it is to be dissipated due to the PMHS losses (see Fig. 1c for a schematic diagram). Amongst other techniques to measure spin-waves⁴, the use of CMP is a particularly simple approach which exploits the sensitivity of microwave technology and transfers it to the detection of magnons. The strong coupling makes the energy stored in a cavity dependent on the one in the material, so an antenna coupled to the electromagnetic field of the cavity gives a simple access to the features of the spin system⁴⁴. Nowadays electronics is extremely developed, and the detection of electromagnetic radiation has been brought to the standard quantum limit of linear amplifiers. At microwave frequencies, Josephson Parametric Amplifiers (JPA) were demonstrated to be the best devices to

^{a)}Electronic mail: nicolo.crescini@phd.unipd.it

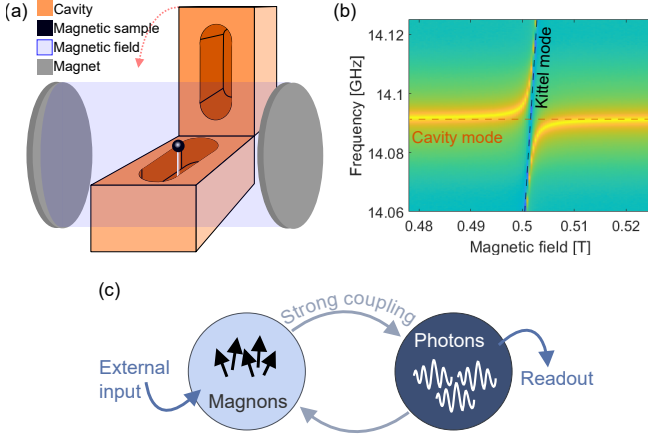


FIG. 1. Schematic representation of a typical PMHS (a), anticrossing curve (b), and diagram of a spin-magnetometer working principle (c). Part (a) represents a PMHS consisting in a YIG sphere housed in a microwave cavity under a static magnetic field. Plot (b) is measured with a .5 mm-diameter YIG sphere in a 14 GHz copper cavity, the colour scale is in logarithmic arbitrary units, where blue to yellow is low to high transmission, and the dashed lines show the uncoupled cavity and Kittel modes.

measure tiniest amounts of power⁴⁵. Thanks to CMPs, such precision can be shifted to a magnetic measurement, as the electromagnetic power in the cavity is highly dependent on the magnetisation of the sample when the coupling strength largely exceeds the system dissipations $g_{cm} \gg \gamma_m, \gamma_c$. It follows that, under these conditions, the quantum-limited readout of a JPA can be exploited to detect spin excitations.

At microwave frequencies, measuring a sample's magnetization becomes increasingly difficult because of technological limitations and fundamental problems, like for example radiation damping^{46–48}. In free space, radiation damping consists in the magnetic dipole emission of a magnetised sample which, at GHz frequencies, drastically decreases the coherence time, limiting the experimental sensitivity. This effect is avoided in PMHSs, as the sample is housed in a resonant cavity which removes the damping by inhibiting the phase space of the emission⁴⁹.

For all their characteristics, PMHSs emerge as an outstanding platform for precision magnetic measurement, which are of interest for a broad range of applications as well as for approaching fundamental physics issues. Hereafter, we describe two types of spin-magnetometers which can be designed with hybrid systems, detail their design and report on their operation. We notice that a high occupation number of the modes permits to treat them as classical oscillators, which is often the case throughout this work, so we rely on a classical treatment of the fields. These devices are originally meant to measure tiniest oscillation of a sample's magnetization, related for example to a Dark Matter Axion field^{49,50}, but can be used to assess many other physical phenomena.

Transverse spin-magnetometer (TSM). - Let's now focus on a hybrid system like the one of in Fig. 1, where a magnetised YIG sphere is placed in a microwave cavity. If an oscillating electromagnetic, or pseudo-electromagnetic, field \mathbf{b}_1 is

oriented perpendicularly to the static field, its quanta can be absorbed by the hybrid magnetic mode. As the magnetization vector \mathbf{M} precesses over the static field, an excitation lying on the precession plane can resonantly interact with it, and the system evolves according to Bloch equations

$$\frac{d\mathbf{M}}{dt} = \gamma(\mathbf{M} \times \mathbf{b}_1)_\perp + \frac{\mathbf{M}}{T_s}, \quad (1)$$

where $\gamma = (2\pi)28 \text{ GHz/T}$ is the electron gyromagnetic ratio, and T_s is the system relaxation time. The driven magnetization resulting from Eq. (1) is

$$M(t) = \gamma\mu_B n_s T_s \cos(\omega_1 t), \quad (2)$$

where ω_1 is the frequency of \mathbf{b}_1 . In a steady state, the power of \mathbf{b}_1 is absorbed, re-emitted by the magnetization, and rapidly converted into photons thanks to the strong coupling.

The optimal experimental condition is an antenna critically coupled to the cavity, which in steady state can extract up to half of the power deposited by the external field, resulting in

$$P_1 = \gamma\mu_B N_s \omega_1 b_1^2 T_s, \quad (3)$$

where N_s is the number of spins of the hybrid system, and the field frequency ω_1 is on resonance with one of the hybrid modes. To calculate the magnetic sensitivity of the TSM, in Eq. (3) we substitute the deposited power P_1 (in Watts) with the power sensitivity of the readout electronics σ_P (in Watts per unit of bandwidth), and recast the equation to isolate the magnetic field. We obtain the sensitivity of the TSM

$$\sigma_{b_1} = \sqrt{\frac{\sigma_P}{\gamma\mu_B N_s \omega_1 T_s}}, \quad (4)$$

in Tesla per unit of bandwidth, which is the field detectable in 1 second integration time with a unitary signal-to-noise ratio. Eq. (4) also shows that the spin-magnetometer sensitivity increases for larger spin-number and longer hybrid system coherence times. This suggests the use of high quality-factor cavities and samples to get a long T_s , and of a large volume of high spin density magnetic material to increase N_s . In this sense, we found a good compromise in YIG. The scalability of the PMHS is of fundamental importance to obtain an increased sensitivity of the setup, as it is directly related to the increment of N_s . To this aim we design spin-magnetometers based on multi-samples PMHS^{51,52}, embedded in cylindrical cavities. To further boost the magnetic sensitivity, we reduce σ_P by operating the device at milli-Kelvin temperatures, to reduce thermal noises and to consent the use of quantum-limited amplifiers.

Following these directions, we built a TSM whose scheme is reported in Fig. 2a. Its PHMS comprises ten YIG spheres, all of 2.1 mm-diameter, produced in-house. These are biased with a magnetic field supplied by a superconducting magnet, with 7 ppm uniformity over the volume containing the spheres. We realise the PMHS by placing the spheres along the axis of a cylindrical cavity (33 mm-diameter, 65 mm-length) allowing them to couple with the uniform rf magnetic field of the TM10 mode at 10.7 GHz.

The PMHS has been designed to reduce the effects of the magnetic dipole interaction between different spheres and of higher order magnetostatic modes. By removing the degeneracy of the TM110 mode we limit the interference of other cavity modes; this is achieved employing a cavity with a quasi-circular section^{53,54}. To describe this system we used a second quantisation model consisting in four coupled harmonic oscillators. We fit it to the experimental anticrossing curve of Fig. 2b⁵³. We then operate the magnetometer in the frequency band 10.2-10.4 GHz, part of the lower frequency hybrid mode range, as identified by the fit (dashed line in the figure)⁵². The operational range is matched with the working band of our Josephson Parametric Converter (JPC), i.e. a JPA formed by a Josephson ring modulator shunted with four inductances⁵⁵. The JPC tuning is allowed by a small superconducting coil biased with a constant current, as shown Fig. 2c. The dashed lines in Fig. 2c includes the 10.2-10.4 GHz frequency interval, showing that in this range the lower frequency hybrid mode can be monitored with our amplifier. The JPC is screened from external disturbances with different layers of superconducting and μ -metal shields, and we verified that the solenoid providing the static field is not affecting the resonance frequencies of the amplifier.

The noise temperature and gain of the electronics chain has been characterised with the injection of microwave signals of known amplitude in an antenna weakly coupled to the cavity. The effective noise temperature results $T_n \simeq 1$ K, which sets the noise power per unit of bandwidth $\sigma_P = k_B T_n$, where k_B is Boltzmann constant. The contribution of the quantum limit to the noise budget is 0.5 K, and the remaining 0.5 K is consistent with extra noise added by the second-stage amplifier, by the losses of the wires and by the PMHS thermodynamic temperature of ~ 100 mK⁵². The spin number and relaxation time are obtained by fitting our model to the transmission measurements of Fig. 2b. The measurement of σ_P , and of N_s and T_s through the PMHS spectroscopy, allows us to calculate the sensitivity of the TSM using Eq. (4). With the parameters of this setup we obtain a magnetic sensitivity of

$$\sigma_{b_1} = 0.9 \times 10^{-18} \left[\left(\frac{1\text{K}}{T_n} \right) \left(\frac{N_s}{10^{21}} \right) \left(\frac{\omega_1/2\pi}{10.4\text{GHz}} \right) \left(\frac{T_s}{168\text{ns}} \right) \right]^{1/2} \frac{\text{T}}{\sqrt{\text{Hz}}}. \quad (5)$$

That the sensitivity given by Eq. (4) holds if the field to be detected has two characteristics: a coherence time longer than T_s , and a coherence length long enough to comprise all the N_s spins.

In particular, this is the case of the field induced by Dark Matter axions^{49,50}, which at GHz frequencies satisfies both these conditions. We used this TSM with a fixed bandwidth of 5 kHz to search for axions, obtaining a limit on their effective field of 5.5×10^{-19} T with about ten hours of integration⁵². A TSM has the advantage of being sensitive to a (pseudo)magnetic field acting on a sample which is within the volume of a resonant cavity. In such a controlled environment, external electromagnetic disturbances are unlikely to be present, making it an interesting testbed for fundamental physics, which are usually not subjected to such screening.

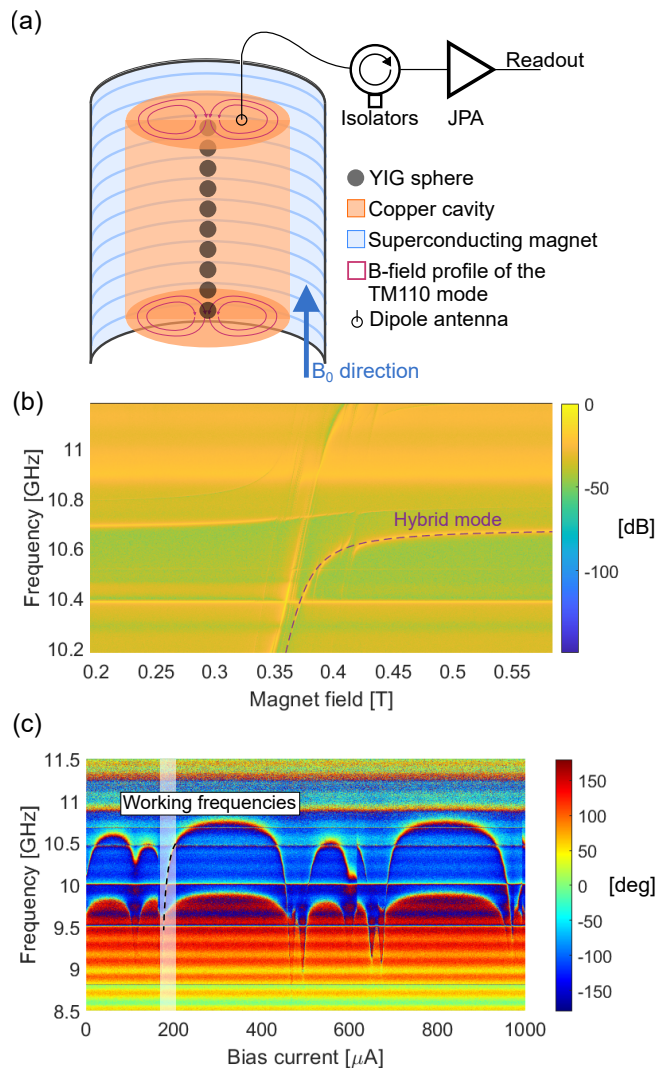


FIG. 2. (a) Simplified scheme of the TSM operated for an axion search⁵² (see text for details). (b) Anticrossing curve of the 10 YIG spheres PMHS, where the dashed line indicates the low-frequency hybrid mode monitored during the measurement. (c) Phase-current diagram of the JPC mounted in this setup, here the dashed line shows the optimal working points of the amplifier. From plots (b) and (c) one notes that the 10.2-10.4 GHz band enables both the PMHS signal transduction and the JPA amplification.

However, from the point of view of the TSM possible technological employment, this feature is a limitation. In fact, the screening due to the cavity makes it difficult to expose the material to a field which is uniform and coherent over the magnetic material volume. Hence, the application of this device is probably limited to the search of new physics.

Longitudinal spin-magnetometer (LSM). - In another possible measurement scheme a persistent oscillating B -field is parallel to the static one. In this configuration, the sample's magnetization precesses about a field $B_0 + b_2 \sin(\omega_2 t)$, where ω_2 and b_2 are the oscillating field frequency and amplitude, and t is time. To illustrate the experimental arrangement, we first consider a simplified scheme including only the mate-

rial and ignoring the presence of the cavity. The experimental scheme is shown in Fig. 3a, where a sphere is surrounded by two crossed loops. Loop number 1 is used to excite the material, while loop number 2 senses the transmitted rf signal, and S_{21} plots are measured. The electron spin resonance (ESR) frequency ω_m of the magnetised sample is modulated at the frequency $\omega_2 \ll \omega_m$ by varying the field $b_2 \ll B_0$. If a monochromatic tone is applied on resonance with ω_m , the effect of b_2 is then to transfer some of the pump power, the carrier, to sidebands at frequencies $\omega_m \pm n\omega_2$, as schematically shown in Fig. 3a for $n = 1$. In the S_{21} spectrum of this simplified system, the amplitude of the first order sideband results

$$\zeta_1 = \frac{\pi A_p^2 Q b_2}{2B_0}, \quad (6)$$

where A_p is the carrier amplitude and $Q = \omega_m/\gamma_m$ the quality factor of the ESR. In a standard ESR technique an externally applied b_2 is used to detect the derivative of the ESR curve with a lock-in amplifier. Here we invert such scheme, and search for oscillating b_2 -fields by sensing the presence of sidebands. The detection of sidebands is limited by the effective noise temperature of the system determining σ_p , the power sensitivity already defined in the case of the TSM. The amplitude ζ_1 is given by Eq. (6) only within the linewidth of the ESR, and drastically reduces for $\omega_2 > \gamma_m$. On the other hand, when $\omega_2 < \gamma_m$, extra noise induced by the pump residual amplitude modulation will increase σ_p . Moreover, at GHz frequencies, radiation damping broadens the linewidth of the ESR, reducing Q . As a consequence, in this configuration the sensitivity for measuring a b_2 field is poor and needs some improvements that can be engineered using PMHSs as follows.

By including a cavity one may consider a PMHS's hybrid mode instead of a bare ESR. CMPs are immune from radiation damping thus we can couple the ESR to a microwave cavity to improve the detection sensitivity. We call ω_p one of the PMHS resonant frequencies: ω_p is also modulated by the oscillating field as $\partial\omega_p/\partial B_0 \simeq r \times \gamma$, where $0 \leq r \leq 1$ is a field-dependent coefficient. When ω_m is equal to the cavity mode resonant frequency, $r = 1/2$. The rf electromagnetic field of the PMHS, pumped with a tone on-resonance with one of the hybrid modes, i. e. at ω_p , is phase-modulated through the variation of the resonant frequency, and therefore produces sidebands too. Their amplitude drastically decreases when they depart from the resonance frequency by several linewidths, but in a PMHS, at the frequency of the second hybrid mode, one sideband does not vanish and hence can be detected (see Fig. 3b). This device is thus sensitive to fields which are at frequencies $\omega_2 \simeq 2g_{cm}$, the splitting of the two hybrid modes. The possibility of detecting the sideband at a frequency much different from the pumping one allows us to drastically reduce the noise by heavily filtering the pump noise. A waveguide is a high pass filter which can cut low frequencies by tens of dB, and that we employ to remove the background related to the pump. If the sideband frequency $\omega_p - \omega_2$ is below the waveguide cut-off, its amplitude is not filtered but the pump noise is (see the electronic scheme in Fig. 3b). By assuming that the carrier noise can be made lower than thermal fluctuations,

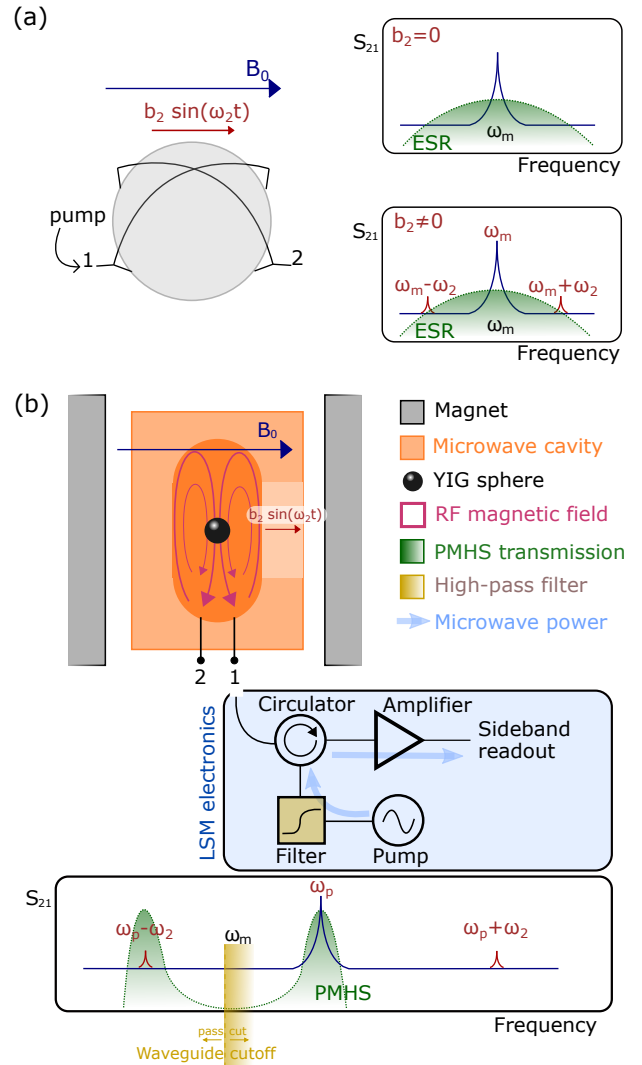


FIG. 3. Schematic explanation of the LSM working principles. (a) Usual design used for the detection of an ESR in a magnetic material consisting in a spherical sample (grey) surrounded by two loops in free space. The rf is fed into the system by loop antenna 1 and the output is read with the perpendicular loop 2. A pump, shown as a blue line in the spectra, is applied on-resonance with the ESR curve (green areas in the S_{21} spectra). In absence of other fields the result is a single peak (left plot), while with a superimposed oscillating field the phase of the carrier is modulated by the shifting of the ESR induced by $b_2 \sin(\omega_2 t)$. Two sidebands, reported in dark red in the right plot, appear at $\omega_m \pm \omega_2$. (b) In the LSM a microwave tone is applied at the frequency of an hybrid mode, while the detection of a sideband, on-resonance with the second mode, probes the presence of b_2 -like fields. The picture shows our room-temperature pilot setup, comprising a YIG sphere and a perforated cavity which allows for the calibration of the spin-magnetometer. Numbers 1 and 2 are two antennas coupled to the cavity, and the side of the cavity coloured in light orange represent a hole housing a loop used for calibration. See text for further details.

the latter becomes the fundamental limitation to the apparatus sensitivity. The magnetic sensitivity can be calculated by rephrasing Eq. (6), and substituting ζ_1 (the sideband power)

with the readout sensitivity σ_P to obtain

$$\sigma_{b_2} = \frac{2B_0}{\pi r Q} \sqrt{\frac{\sigma_P}{A_p^2}}, \quad (7)$$

where, in this case, Q is the quality factor of the hybrid mode. From Eq. (7) one can see that the carrier power A_p^2 can be arbitrarily increased to improve the LSM magnetic sensitivity, assuming that its noise can be reduced consequently. With realistic parameters of our PMHS, one can estimate the sensitivity of a room-temperature LSM with Eq. (7), resulting in

$$\sigma_{b_2} = 10.4 \left(\frac{B_0}{0.4\text{T}} \right) \left(\frac{Q}{10^4} \right) \sqrt{\left(\frac{A_n^2/k_B}{300\text{K}} \right) \left(\frac{100\text{mW}}{A_p^2} \right)} \frac{\text{fT}}{\sqrt{\text{Hz}}}, \quad (8)$$

which is already competitive with state-of-the-art magnetometers like superconducting quantum interference devices (SQUIDs)^{56–60} or spin-exchange relaxation-free (SERFs)^{61–63}. Interestingly, σ_{b_2} does not depend on any extensive parameter, in contrast with σ_{b_1} which relies on the total number of spins. This means that the LSM can in principle be miniaturised without compromising its sensitivity, and removing the need of detecting a uniform field over a large volume.

A room-temperature prototype was devised to test the actual functioning of this device, and a scheme of the setup is reported in Fig. 3b. The number of spins in the sphere, together with the shape of the rf-magnetic field of the cavity mode, set the magnetometer working frequency $\omega_2 \simeq (2\pi) 200\text{MHz}$. The cavity mode and the ESR resonate at 11.5 GHz (corresponding to $B_0 = 0.4\text{T}$), and their linewidths determine the overall quality factor of the hybrid mode $Q = 2750$, which is approximately the average of the two. An antenna with variable coupling is connected to the cavity to inject and extract power from the hybrid system through a circulator. A microwave pump on resonance with the high-frequency hybrid mode at ω_p is filtered with a waveguide before being injected in the PMHS, obtaining the input power $A_p^2 = 0.2\text{mW}$. The signal to be detected is the PMHS output power of the sideband at $\omega_p - \omega_2$, the lower hybrid mode frequency. At $\omega_p - \omega_2$, the background is mainly thermal thanks to the filtering waveguide. The extracted signal is amplified with a low noise HEMT before being acquired with a spectrum analyser, and the whole electronic chain has been characterised by injecting calibrated signals. The readout noise results $\sigma_P \simeq 4 \times 10^{-21} \text{W/Hz}$, mostly due to room temperature thermodynamic fluctuations, and two orders of magnitude lower than the pump noise, showing that our configuration almost removes the tone-induced background. To calibrate the magnetic sensitivity of the device, we inject pico-Tesla fields at 200 MHz using a single loop on one side of the cavity, which generates a known field parallel to B_0 on the YIG sphere (see Fig. 3b). The setup was not optimized, but the expected losses due to imperfect matchings can be measured and accounted for by a factor $k = 2.1$, lowering the LSM sensitivity. With these quantities, from Eq. (7), the expected sensitivity of the apparatus results $k\sigma_{b_2} = 1.9\text{pT}/\sqrt{\text{Hz}}$. The prototype was calibrated with fields ranging from 2 to 14 pT and shows a mea-

sured sensitivity of $2.0 \pm 0.4\text{pT}/\sqrt{\text{Hz}}$, compatible with the estimated value⁶⁴. In this setup the loop on the side of the cavity was used for calibration, but in principle, it can be an input coil which transduces a field to the sensitive element of the magnetometer (the magnetic sphere). This signal transduction is similar to what is usually done with SQUIDs, where an input coil is coupled to the junctions loop. From Eq. (7), one notices that the LSM magnetic sensitivity benefits from high quality factors, low readout noise, and high pump power. The former feature is related to the quality factors of the PMHS, which should comprise narrow-linewidth cavities and magnetic materials to improve the magnetometer sensitivity. The latter two essentially depend on the microwave electronics of the setup. Since the sensitivity is size-independent, miniaturisation can be foreseen by using 2D printed resonators and small quantities of material. Eventually, we mention that multiplexing was also shown to be a viable option in similar devices^{65–67}.

The sensitivity of the two PMHS-based magnetometers is limited by the noise of the readout noise temperature, which ultimately consists in quantum fluctuations⁶⁸. We foresee the use of broadband Travelling Wave JPA^{69–71} to overcome the standard JPA limitation of being resonant. To overcome the quantum-limit one may rely on single photon or magnon counters, which are unaffected by this issue, rather than on linear amplifiers.

A downside of both the magnetometers is that their resonant nature implies a reduced bandwidth, limited to the linewidth of an hybrid mode. Nevertheless, as the resonant frequencies of the hybrid modes can be changed with a tuning of the B_0 field, the band of both the TSM and LSM can be extended. In particular, for TSMs this changes the hybrid mode frequency (see Fig. 2b), and for LSMs is a variation of the vacuum-Rabi splitting $2g_{cm}$. Since the working band of the two magnetometers is controlled by the dynamics of CMPs, the latter was studied in a separate work⁷².

In conclusion, we described and operated two different types of CMP-based magnetometers, which show an outstanding magnetic sensitivity. The TSM is a device that benefits from its scalability, which lowers the minimum detectable magnetization oscillations. We believe that it is more suitable for studying fundamental physics, for instance in the search for Axions, where Dark Matter can be described as a wide, uniform, and persistent rf field acting on the electron spins. The LSM is a device of simpler application, as it can precisely detect faint magnetic fields localised on a small spin ensemble. Its sensitivity relies on the design and engineering of the PMHS, which can be further developed to reach remarkable sensitivity improvements. We mention that its usage to search for Axions is immediate, and that a single LSM can scan a broad Axion-mass range by changing the CMP vacuum-Rabi splitting. We showed that the unique features of PMHS makes them suitable to assess fundamental physics problems, and we envision more future applications of these systems as testbeds for precision magnetometry.

ACKNOWLEDGMENTS

The authors would like to acknowledge the contribution of the QUAX collaboration in the development of these devices. We also thank Enrico Berto, Andrea Benato, Fulvio Calaan, and Mario Tessaro for the help in the building of the experimental setups, and in particular for the aid with the mechanics, cryogenics, and electronics of the apparatuses. We acknowledge the support of INFN-Laboratori Nazionali di Legnaro, for hosting all the experimental setups described in this work, and for the availability of large quantities of liquid helium.

DATA AVAILABILITY

The data supporting the findings of this work are available from the corresponding author upon reasonable request.

- ¹A. A. Clerk, K. W. Lehnert, P. Bertet, J. R. Petta, and Y. Nakamura, “Hybrid quantum systems with circuit quantum electrodynamics,” *Nature Physics* **16**, 257–267 (2020).
- ²D. Lachance-Quirion, Y. Tabuchi, A. Gloppe, K. Usami, and Y. Nakamura, “Hybrid quantum systems based on magnonics,” *Applied Physics Express* **12**, 070101 (2019).
- ³S. Haroche and J.-M. Raimond, *Exploring the Quantum: Atoms, Cavities, and Photons* (Oxford University Press, 2006).
- ⁴A. V. Chumak, V. I. Vasyuchka, A. A. Serga, and B. Hillebrands, “Magnon spintronics,” *Nature Physics* **11**, 453–461 (2015).
- ⁵C. L. Degen, F. Reinhard, and P. Cappellaro, “Quantum sensing,” *Rev. Mod. Phys.* **89**, 035002 (2017).
- ⁶G. Kurizki, P. Bertet, Y. Kubo, K. Mølmer, D. Petrosyan, P. Rabl, and J. Schmiedmayer, “Quantum technologies with hybrid systems,” *Proceedings of the National Academy of Sciences* **112**, 3866–3873 (2015), <http://www.pnas.org/content/112/13/3866.full.pdf>.
- ⁷Y. R. Shen and N. Bloembergen, “Interaction between light waves and spin waves,” *Phys. Rev.* **143**, 372–384 (1966).
- ⁸C. Kittel, *Introduction to Solid State Physics*, 8th ed. (Wiley, 2004).
- ⁹D. F. Walls and G. J. Milburn, *Quantum optics* (Springer Science & Business Media, 2007).
- ¹⁰Y. Tabuchi, S. Ishino, A. Noguchi, T. Ishikawa, R. Yamazaki, K. Usami, and Y. Nakamura, “Quantum magnonics: The magnon meets the superconducting qubit,” *Comptes Rendus Physique* **17**, 729 – 739 (2016), quantum microwaves / Micro-ondes quantiques.
- ¹¹X. Zhang, C.-L. Zou, N. Zhu, F. Marquardt, L. Jiang, and H. X. Tang, “Magnon dark modes and gradient memory,” *Nature Communications* **6**, 8914 (2015).
- ¹²D. I. Schuster, A. P. Sears, E. Ginossar, L. DiCarlo, L. Frunzio, J. J. L. Morton, H. Wu, G. A. D. Briggs, B. B. Buckley, D. D. Awschalom, and R. J. Schoelkopf, “High-cooperativity coupling of electron-spin ensembles to superconducting cavities,” *Phys. Rev. Lett.* **105**, 140501 (2010).
- ¹³A. Ghirri, C. Bonizzoni, D. Gerace, S. Sanna, A. Cassinese, and M. Affronte, “Ybco microwave resonators for strong collective coupling with spin ensembles,” *Applied Physics Letters*, **106** (2015).
- ¹⁴O. O. Soykal and M. E. Flatté, “Strong field interactions between a nano-magnet and a photonic cavity,” *Phys. Rev. Lett.* **104**, 077202 (2010).
- ¹⁵A. Ghirri, C. Bonizzoni, F. Troiani, N. Buccheri, L. Beverina, A. Cassinese, and M. Affronte, “Coherently coupling distinct spin ensembles through a high- t_c superconducting resonator,” *Physical Review A*, **93** (2016).
- ¹⁶K. Heshami, D. G. England, P. C. Humphreys, P. J. Bustard, V. M. Acosta, J. Nunn, and B. J. Sussman, “Quantum memories: emerging applications and recent advances,” *Journal of Modern Optics* **63**, 2005–2028 (2016), <https://doi.org/10.1080/09500340.2016.1148212>.
- ¹⁷H. J. Kimble, “The quantum internet,” *Nature* **453**, 1023–1030 (2008).
- ¹⁸L. A. Williamson, Y.-H. Chen, and J. J. Longdell, “Magneto-optic modulator with unit quantum efficiency,” *Phys. Rev. Lett.* **113**, 203601 (2014).
- ¹⁹X. Fernandez-Gonzalvo, Y.-H. Chen, C. Yin, S. Rogge, and J. J. Longdell, “Coherent frequency up-conversion of microwaves to the optical telecommunications band in an er:ysio crystal,” *Phys. Rev. A* **92**, 062313 (2015).
- ²⁰R. Hisatomi, A. Osada, Y. Tabuchi, T. Ishikawa, A. Noguchi, R. Yamazaki, K. Usami, and Y. Nakamura, “Bidirectional conversion between microwave and light via ferromagnetic magnons,” *Phys. Rev. B* **93**, 174427 (2016).
- ²¹C. Braggio, G. Carugno, M. Guarise, A. Ortolan, and G. Ruoso, “Optical manipulation of a magnon-photon hybrid system,” *Physical Review Letters*, **118** (2016).
- ²²D. Lachance-Quirion, Y. Tabuchi, S. Ishino, A. Noguchi, T. Ishikawa, R. Yamazaki, and Y. Nakamura, “Resolving quanta of collective spin excitations in a millimeter-sized ferromagnet,” *Science Advances* **3** (2017), 10.1126/sciadv.1603150, <https://advances.sciencemag.org/content/3/7/e1603150.full.pdf>.
- ²³D. Lachance-Quirion, S. P. Wolski, Y. Tabuchi, S. Kono, K. Usami, and Y. Nakamura, “Entanglement-based single-shot detection of a single magnon with a superconducting qubit,” *Science* **367**, 425–428 (2020), <https://science.sciencemag.org/content/367/6476/425.full.pdf>.
- ²⁴S. P. Wolski, D. Lachance-Quirion, Y. Tabuchi, S. Kono, A. Noguchi, K. Usami, and Y. Nakamura, “Dissipation-based quantum sensing of magnons with a superconducting qubit,” (2020), arXiv:2005.09250 [quant-ph].
- ²⁵C. M. Bender, “Making sense of non-hermitian hamiltonians,” *Reports on Progress in Physics* **70**, 947–1018 (2007).
- ²⁶C. M. Bender and S. Boettcher, “Real spectra in non-hermitian hamiltonians having pt symmetry,” *Phys. Rev. Lett.* **80**, 5243–5246 (1998).
- ²⁷C. E. Rüter, K. G. Makris, R. El-Ganainy, D. N. Christodoulides, M. Segev, and D. Kip, “Observation of parity–time symmetry in optics,” *Nature Physics* **6**, 192–195 (2010).
- ²⁸D. Zhang, X.-Q. Luo, Y.-P. Wang, T.-F. Li, and J. Q. You, “Observation of the exceptional point in cavity magnon-polaritons,” *Nature Communications* **8**, 1368 (2017).
- ²⁹X. Zhang, K. Ding, X. Zhou, J. Xu, and D. Jin, “Experimental observation of an exceptional surface in synthetic dimensions with magnon polaritons,” *Phys. Rev. Lett.* **123**, 237202 (2019).
- ³⁰K. Ding, G. Ma, M. Xiao, Z. Q. Zhang, and C. T. Chan, “Emergence, coalescence, and topological properties of multiple exceptional points and their experimental realization,” *Phys. Rev. X* **6**, 021007 (2016).
- ³¹G.-Q. Zhang and J. Q. You, “Higher-order exceptional point in a cavity magnonics system,” *Phys. Rev. B* **99**, 054404 (2019).
- ³²Y. Cao and P. Yan, “Exceptional magnetic sensitivity of \mathcal{PT} -symmetric cavity magnon polaritons,” *Phys. Rev. B* **99**, 214415 (2019).
- ³³J. W. Rao, S. Kaur, B. M. Yao, E. R. J. Edwards, Y. T. Zhao, X. Fan, D. Xue, T. J. Silva, Y. S. Gui, and C.-M. Hu, “Analogue of dynamic hall effect in cavity magnon polariton system and coherently controlled logic device,” *Nature Communications* **10**, 2934 (2019).
- ³⁴N. J. Lambert, J. A. Haigh, S. Langenfeld, A. C. Doherty, and A. J. Ferguson, “Cavity-mediated coherent coupling of magnetic moments,” *Phys. Rev. A* **93**, 021803 (2016).
- ³⁵Y.-P. Wang, J. W. Rao, Y. Yang, P.-C. Xu, Y. S. Gui, B. M. Yao, J. Q. You, and C.-M. Hu, “Nonreciprocity and unidirectional invisibility in cavity magnonics,” *Phys. Rev. Lett.* **123**, 127202 (2019).
- ³⁶Y.-P. Wang, G.-Q. Zhang, D. Zhang, T.-F. Li, C.-M. Hu, and J. Q. You, “Bistability of cavity magnon polaritons,” *Phys. Rev. Lett.* **120**, 057202 (2018).
- ³⁷H. Y. Yuan, P. Yan, S. Zheng, Q. Y. He, K. Xia, and M.-H. Yung, “Steady bell state generation via magnon-photon coupling,” *Phys. Rev. Lett.* **124**, 053602 (2020).
- ³⁸H. Huebl, C. W. Zollitsch, J. Lotze, F. Hocke, M. Greifenstein, A. Marx, R. Gross, and S. T. B. Goennenwein, “High cooperativity in coupled microwave resonator ferrimagnetic insulator hybrids,” *Phys. Rev. Lett.* **111**, 127003 (2013).
- ³⁹Y. Tabuchi, S. Ishino, T. Ishikawa, R. Yamazaki, K. Usami, and Y. Nakamura, “Hybridizing ferromagnetic magnons and microwave photons in the quantum limit,” *Phys. Rev. Lett.* **113**, 083603 (2014).
- ⁴⁰X. Zhang, C.-L. Zou, L. Jiang, and H. X. Tang, “Strongly coupled magnons and cavity microwave photons,” *Phys. Rev. Lett.* **113**, 156401 (2014).
- ⁴¹M. Goryachev, W. G. Farr, D. L. Creedon, Y. Fan, M. Kostylev, and M. E. Tobar, “High-cooperativity cavity qed with magnons at microwave frequen-

- cies,” *Phys. Rev. Applied* **2**, 054002 (2014).
- ⁴²D. Zhang, X.-M. Wang, T.-F. Li, X.-Q. Luo, W. Wu, F. Nori, and J. Q. You, “Cavity quantum electrodynamics with ferromagnetic magnons in a small yttrium-iron-garnet sphere,” *npj Quantum Information* **1**, 15014 (2015).
- ⁴³Y. Tabuchi, S. Ishino, A. Noguchi, T. Ishikawa, R. Yamazaki, K. Usami, and Y. Nakamura, “Coherent coupling between a ferromagnetic magnon and a superconducting qubit,” *Science* **349**, 405–408 (2015), <https://science.sciencemag.org/content/349/6246/405.full.pdf>.
- ⁴⁴T. Wolz, A. Stehli, A. Schneider, I. Bovenster, R. Macêdo, A. V. Ustinov, M. Kläui, and M. Weides, “Introducing coherent time control to cavity magnon-polariton modes,” *Communications Physics* **3**, 3 (2020).
- ⁴⁵A. Roy and M. Devoret, “Introduction to parametric amplification of quantum signals with josephson circuits,” *Comptes Rendus Physique* **17**, 740–755 (2016), quantum microwaves / Micro-ondes quantiques.
- ⁴⁶S. Bloom, “Effects of radiation damping on spin dynamics,” *Journal of Applied Physics* **28**, 800–805 (1957).
- ⁴⁷M. Augustine, “Transient properties of radiation damping,” *Progress in Nuclear Magnetic Resonance Spectroscopy* **40**, 111–150 (2002).
- ⁴⁸N. Bloembergen and R. V. Pound, “Radiation damping in magnetic resonance experiments,” *Phys. Rev.* **95**, 8–12 (1954).
- ⁴⁹R. Barbieri, C. Braggio, G. Carugno, C. Gallo, A. Lombardi, A. Ortolan, R. Pengo, G. Ruoso, and C. Speake, “Searching for galactic axions through magnetized media: The quax proposal,” *Physics of the Dark Universe* **15**, 135–141 (2017).
- ⁵⁰R. Barbieri, M. Cerdonio, G. Fiorentini, and S. Vitale, “Axion to magnon conversion. a scheme for the detection of galactic axions,” *Physics Letters B* **226**, 357–360 (1989).
- ⁵¹Crescini, N., Alesini, D., Braggio, C., Carugno, G., Di Gioacchino, D., Gallo, C. S., Gambardella, U., Gatti, C., Iannone, G., Lamanna, G., Ligi, C., Lombardi, A., Ortolan, A., Pagano, S., Pengo, R., Ruoso, G., Speake, C. C., and Taffarello, L., “Operation of a ferromagnetic axion haloscope at $m_a = 58 \mu\text{eV}$,” *Eur. Phys. J. C* **78**, 703 (2018).
- ⁵²N. Crescini, D. Alesini, C. Braggio, G. Carugno, D. D’Agostino, D. Di Gioacchino, P. Falferi, U. Gambardella, C. Gatti, G. Iannone, C. Ligi, A. Lombardi, A. Ortolan, R. Pengo, G. Ruoso, and L. Taffarello (QUAX Collaboration), “Axion search with a quantum-limited ferromagnetic haloscope,” *Phys. Rev. Lett.* **124**, 171801 (2020).
- ⁵³N. Crescini, C. Braggio, G. Carugno, A. Ortolan, and G. Ruoso, “Coherent coupling between multiple ferrimagnetic spheres and a microwave cavity in the quantum-limit,” (2020), [arXiv:2007.08908](https://arxiv.org/abs/2007.08908) [quant-ph].
- ⁵⁴R. Macêdo, R. C. Holland, P. G. Baity, K. L. Livesey, R. L. Stamps, M. P. Weides, and D. A. Bozhko, “An electromagnetic approach to cavity spintronics,” (2020), [arXiv:2007.11483](https://arxiv.org/abs/2007.11483) [quant-ph].
- ⁵⁵N. Roch, E. Flurin, F. Nguyen, P. Morfin, P. Campagne-Ibarcq, M. H. Devoret, and B. Huard, “Widely tunable, nondegenerate three-wave mixing microwave device operating near the quantum limit,” *Phys. Rev. Lett.* **108**, 147701 (2012).
- ⁵⁶R. C. Jaklevic, J. Lambe, A. H. Silver, and J. E. Mercereau, “Quantum interference effects in josephson tunneling,” *Phys. Rev. Lett.* **12**, 159–160 (1964).
- ⁵⁷S. N. Erné, H. Hahlbohm, and H. Lübbig, “Theory of rf-biased superconducting quantum interference device for nonhysteretic regime,” *Journal of Applied Physics* **47**, 5440–5442 (1976), <https://doi.org/10.1063/1.322574>.
- ⁵⁸M. Aprili, “The nanosquid makes its debut,” *Nature Nanotechnology* **1**, 15–16 (2006).
- ⁵⁹R. Kleiner, D. Koelle, F. Ludwig, and J. Clarke, “Superconducting quantum interference devices: State of the art and applications,” *Proceedings of the IEEE* **92**, 1534–1548 (2004).
- ⁶⁰C. John and B. Alex I., *The SQUID Handbook* (John Wiley & Sons, Ltd, 2005) <https://onlinelibrary.wiley.com/doi/pdf/10.1002/3527603646.fmatter>.
- ⁶¹I. K. Kominis, T. W. Kornack, J. C. Allred, and M. V. Romalis, “A subfemtotesla multichannel atomic magnetometer,” *Nature* **422**, 596–599 (2003).
- ⁶²I. M. Savukov, S. J. Seltzer, M. V. Romalis, and K. L. Sauer, “Tunable atomic magnetometer for detection of radio-frequency magnetic fields,” *Phys. Rev. Lett.* **95**, 063004 (2005).
- ⁶³D. Budker and M. Romalis, “Optical magnetometry,” *Nature Physics* **3**, 227–234 (2007).
- ⁶⁴N. Crescini, G. Ruoso, and G. Carugno, “In preparation,” (2020).
- ⁶⁵S. Kempf, M. Wegner, A. Fleischmann, L. Gastaldo, F. Herrmann, M. Papst, D. Richter, and C. Enss, “Demonstration of a scalable frequency-domain readout of metallic magnetic calorimeters by means of a microwave squid multiplexer,” *AIP Advances* **7**, 015007 (2017), <https://doi.org/10.1063/1.4973872>.
- ⁶⁶K. D. Irwin and K. W. Lehnert, “Microwave squid multiplexer,” *Applied Physics Letters* **85**, 2107–2109 (2004), <https://doi.org/10.1063/1.1791733>.
- ⁶⁷J. A. B. Mates, G. C. Hilton, K. D. Irwin, L. R. Vale, and K. W. Lehnert, “Demonstration of a multiplexer of dissipationless superconducting quantum interference devices,” *Applied Physics Letters* **92**, 023514 (2008), <https://doi.org/10.1063/1.2803852>.
- ⁶⁸S. K. Lamoreaux, K. A. van Bibber, K. W. Lehnert, and G. Carosi, “Analysis of single-photon and linear amplifier detectors for microwave cavity dark matter axion searches,” *Phys. Rev. D* **88**, 035020 (2013).
- ⁶⁹A. L. Cullen, “A travelling-wave parametric amplifier,” *Nature* **181**, 332–332 (1958).
- ⁷⁰C. Macklin, K. O’Brien, D. Hover, M. E. Schwartz, V. Bolkhovsky, X. Zhang, W. D. Oliver, and I. Siddiqi, “A near-quantum-limited josephson traveling-wave parametric amplifier,” *Science* **350**, 307–310 (2015), <https://science.sciencemag.org/content/350/6258/307.full.pdf>.
- ⁷¹L. Planat, A. Ranadive, R. Dassonneville, J. Puertas Martínez, S. Léger, C. Naud, O. Buisson, W. Hasch-Guichard, D. M. Basko, and N. Roch, “Photonic-crystal josephson traveling-wave parametric amplifier,” *Phys. Rev. X* **10**, 021021 (2020).
- ⁷²N. Crescini, C. Braggio, G. Carugno, R. Di Vora, A. Ortolan, and G. Ruoso, “Magnon-driven dynamics of a hybrid system excited with ultrafast optical pulses,” *Communications Physics* **3**, 164 (2020).